Proc. Natl. Acad. Sci. USA
Vol. 93, pp. 2382–2386, March 1996
Neurobiology

Mapping striate and extrastriate visual areas in human cerebral cortex

EDGAR A. DEYOE*, GEORGE J. CARMAN†, PETER BANDETTINI‡, SETH GLICKMAN*, JON WIESER*, ROBERT COX§, DAVID MILLER¶, AND JAY NEITZ*

*Department of Cellular Biology and Anatomy, and Biophysics Research Institute, The Medical College of Wisconsin, 8701 Watertown Plank Road, Milwaukee, WI 53226; †The Salk Institute for Biological Studies, La Jolla, CA 92037; ‡Massachusetts General Hospital–NMR Center, Charlestown, MA 02129; §Biophysics Research Institute, The Medical College of Wisconsin, Milwaukee, WI 53226; and ¶Brown University, Providence, RI 02912

Communicated by Francis Crick, The Salk Institute for Biological Sciences, San Diego, CA, November 14, 1995 (received for review August 2, 1995)

ABSTRACT **Functional magnetic resonance imaging (fMRI) was used to identify and map the representation of the visual field in seven areas of human cerebral cortex and to identify at least two additional visually responsive regions. The cortical locations of neurons responding to stimulation along the vertical or horizontal visual field meridia were charted on three-dimensional models of the cortex and on unfolded maps of the cortical surface. These maps were used to identify the borders among areas that would be topographically homologous to areas V1, V2, V3, VP, and parts of V3A and V4 of the macaque monkey. Visually responsive areas homologous to the middle temporal/medial superior temporal area complex and unidentified parietal visual areas were also observed. The topography of the visual areas identified thus far is consistent with the organization in macaque monkeys. However, these and other findings suggest that human and simian cortical organization may begin to differ in extrastriate cortex at, or beyond, V3A and V4.**

In contrast to our extensive knowledge of cortical organization in nonhuman primates, far less is known about the identity and topography of functional subdivisions in human cerebral cortex. In the macaque monkey cortex, 30 or more distinct visual areas have been tentatively identified (1). In the human brain, a strong case has been made for only two or three areas (V1, V2, and middle temporal) (2, 4–6), though several additional areas have been proposed (6–11). Brain images produced by functional magnetic resonance imaging (fMRI) show signals that are thought to represent local changes in blood oxygenation. These changes can be elicited by sensory-evoked neural activity though other factors such as alterations in blood volume and proton movement may also contribute [for review, see DeYoe *et al.* (12)]. We have used this technology to chart several functionally distinct visual areas in the human. Preliminary reports of this work have appeared (13, 14).

MATERIALS AND METHODS

To map angular positions within the visual field, four male and two female subjects (ages 24–40 years old) viewed a flickering black-and-white-checkered hemifield that rotated slowly about a central fixation point during a fMRI scan. To map visual field eccentricity (distance from the center of gaze), subjects viewed an expanding checkered annulus. In this manner, neurons responding to stimulation at different locations in the visual field were activated at different times during the stimulus sequence. Corresponding differences in the temporal phase of the fMRI response thus identified the retinotopic location represented by each active site in the brain (12). A similar technique has been described by Engel *et al.* (15).

To enhance activation of extrastriate cortex (12) and to help maintain attention and arousal, the subject was required to detect a small target appearing at a random position superimposed on the checkered hemifield or annulus. A new target was presented every 2 sec and the subject activated one of two switches to indicate the direction of change in location of the target (closer or farther from the center for the hemifield or closer or farther from the 12 o'clock position for the annuli).

Details of procedures for fMRI have been published (12). Briefly, a General Electric Signa MRI scanner equipped with a custom head coil (16) and custom optical system (17) was used to acquire sets of gradient-recalled (TE = 40 msec; TR = 2000 msec) echo-planar images of 10–20 slices through the brain every 2 sec while the subject performed the visual discrimination task. Two to four repetitions of the sequence were averaged to increase contrast-to-noise ratio. For three of the six subjects, both spin echo images (TE = 100 msec; TR = 2000 msec) and gradient-recalled images were obtained simultaneously. Results obtained with both methods were consistent, though spin-echo sequences were less sensitive and had less high spatial frequency noise.

Valid response foci were detected in the fMRI images by using a temporal cross-correlation analysis (12, 18). A statistical criterion ensuring less than 1 false positive per 1000–10,000 image pixels was determined from the sampling distribution of the cross-correlations for blank trials corrected for multiple comparisons (19).

Surface models of each subject's occipital lobes were constructed from tracings of the gray/white matter boundary in T1-weighted spoiled GRASS (gradient-recalled at steady state) images. The traced contours were combined into a triangularly tessellated surface by using NUAGES software (20). The surface was then expanded outward along the surface normals by half the average cortical thickness (1.42 mm) to approximate cortical layer 4. For each pixel in the fMRI images, the response amplitude was assigned to the single nearest point on the reconstructed surface. It was also assigned to neighboring points within a radius proportional to half the size of an imaging voxel (typically, 3.75 × 3.75 × 4.0 mm). The complete pattern was then smoothed by a weighted average of the activity at each node and its neighbors.

Finally, a "flattening" algorithm (21) was used to computationally unfold the surface model thereby yielding a two-dimensional flat map of the cortex with the associated activation patterns. Due to the optimization provided by this algorithm, distances between points on the two-dimensional surface matched the distances on the original three-dimensional surface with an average error of 15% or less. The triangular

The publication costs of this article were defrayed in part by page charge payment. This article must therefore be hereby marked "*advertisement*" in accordance with 18 U.S.C. §1734 solely to indicate this fact.

Abbreviation: fMRI, functional magnetic resonance imaging.

tessellation of the surface also preserved angular relationships among points.

RESULTS

Fig. 1 illustrates the cortical activity evoked in three subjects by the expanding ring stimuli. Annuli of increasing eccentricity from the fixation point evoked bands of activity that cut across the medial and ventral surfaces of the occipital lobe. The foveal representation was located posteriorly near the pole and greater eccentricities were represented anteriorly. The bands extended from the collateral sulcus ventrally, crossed the calcarine fissure and passed dorsally out onto the exposed lateral surface (Fig. 1*A*). Additional foci representing the peripheral visual field were found in dorsal parietal cortex and in the parietooccipital sulcus near the junction with the calcarine sulcus. A separate peripheral representation was observed in or near the lateral occipital sulcus close to the junction of the parietal, temporal, and occipital lobes.

Fig. 2 illustrates results from the rotating hemifield experiments for the same three subjects. Cortex shaded in yellow was maximally activated when the center of the stimulus was within 45° of the superior vertical meridian. Cortex shaded purple or orange was maximally activated for stimulus positions within 45° of the horizontal meridian or the inferior vertical meridian, respectively.

As expected from earlier work, a prominent representation of the horizontal meridian was found within the calcarine fissure. This was flanked dorsally in the cuneus by a representation of the inferior vertical meridian (shown in orange) and then by another horizontal meridian (cf. Fig. 2 *B* and *B'*). The latter was flanked by a second inferior vertical meridian (orange) that extended onto the lateral operculum. In some subjects, a third weak representation of the horizontal meridian could be detected on the lateral surface of the occipital lobe (cf. Fig. 2 *A'* and *B'*). A similar alternation of vertical and horizontal meridian representations was observed in ventral occipital cortex. One representation of the superior vertical meridian was found just below the calcarine sulcus. This was flanked ventrally by another horizontal meridian representation and by a second superior vertical meridian. Again another faint horizontal meridian focus was observed ventrolaterally on the fusiform gyrus in at least one subject (cf. Fig. 2*B'*).

The results illustrated in Figs. 1 and 2 are representative of results from all six subjects. Data from all subjects showed the alternation of visual field meridia as well as the anterior progression of activation as visual field eccentricity increased. Moreover, the individual variability apparent in Figs. 1 and 2 was also qualitatively similar for the other subjects.

Fig. 3*A* summarizes the alternating pattern of meridian representations for all three subjects. Spline curves were fitted by eye to the middle of each major activity band shown in Fig. 2. The spline curves for two of the subjects (Fig. 2 *B* and *C*) were then slightly scaled and rotated (maximum 10% scaling and 5° rotation) and then overlaid on the map of subject A to produce the composite shown in Fig. 3*A*. Fig. 3*C* shows how this was also accomplished for the isoeccentricity bands of Fig. 1 using the same scaling and rotation factors. Finally, a grid representing the mean meridian and isoeccentricity contours for the three subjects is illustrated in Fig. 3*B*.

A common organizational principle of the primate visual system is that the boundaries between retinotopically organized visual areas are often located at, or close to, the cortical representations of the horizontal or vertical meridia (23). Consequently, the meridian representations illustrated in Fig. 3 effectively identify the borders between visual areas in the human. Of the most thoroughly studied subhuman species, the organization of visual areas in macaque monkeys is likely to be close to the organization in humans (24). Accordingly, we have used the layout of macaque visual areas proposed by Felleman and Van Essen (1) as the basis for our proposed arrangement of human visual areas illustrated in Fig. 4.

By comparing Figs. 3 and 4, it can be seen that striate cortex, area V1, occupies the calcarine fissure but extends a variable distance onto the surface of the cuneus and lingual gyrus. The representation of the horizontal meridian (HM1) contained

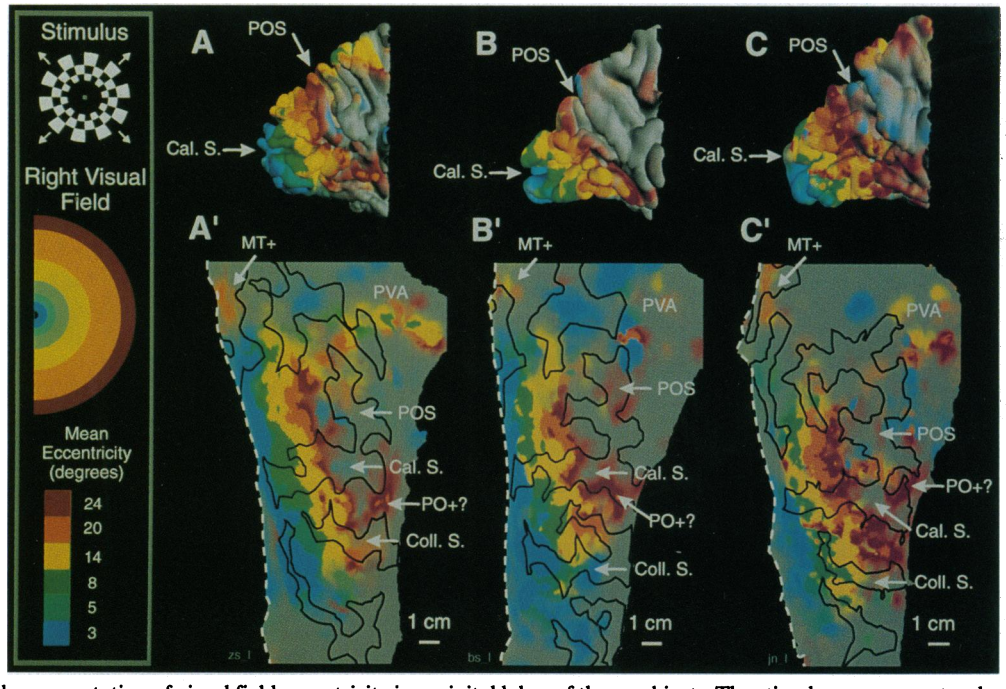

FIG. 1. Cortical representation of visual field eccentricity in occipital lobes of three subjects. The stimulus was a counterphase-flickering (8 Hz) checkered annulus expanding from 1.4° to 24° in 40 sec and was repeated five times during fMRI scan. Step size, check size, and width were scaled in proportion to eccentricity. Maximum outer radius was limited to 30° by optical viewer. Check contrast, 98%; mean luminance, 34.5 cd/m². (*A–C*) Three-dimensional view, medial occipital lobe, anterior to right. (*A'–C'*) Flat maps. Colors (blue to red) represent activation by six groups of three successive annuli. Inclusive eccentricities (degrees): 1.4–4.5, 2.3–7.6, 3.7–12.4, 6.3–20.8, 10.5–30, and 17.1–30, respectively, for *A–C* and *A'–C'*. Coloring of hemifield is only approximate; the true mean eccentricities are shown at the lower left (see Fig. 2 for abbreviations).

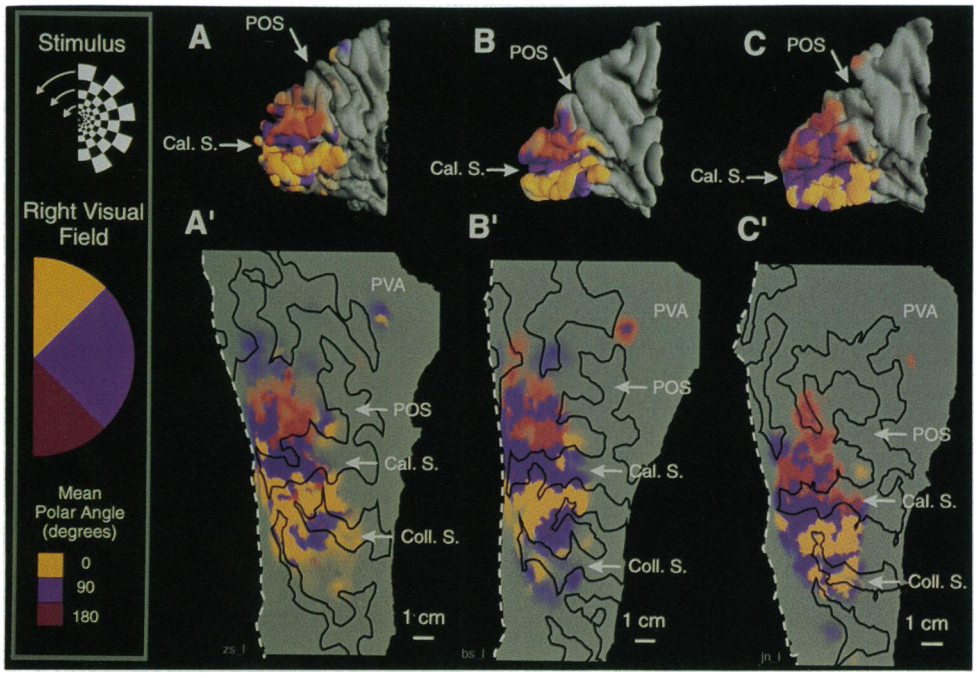

FIG. 2. Cortical representation of visual field quadrants in occipital lobes of three subjects. Subjects, protocol, and layout (*A–C* and *A′–C′*) are the same as for Fig. 1 except the stimulus was a checkered hemifield rotated about the fixation point. Cal. S., calcarine sulcus; Coll. S., collateral sulcus; MT+, middle temporal visual area (see Fig. 1); PO+?, possible parietooccipital area (22); POS, parietooccipital sulcus; PVA, parietal visual areas. White dashed lines on flat maps show margins of slit running from occipital pole along lateral occipital sulcus. Upper and lower halves of dashed line would be juxtaposed in the three-dimensional brain.

within the calcarine fissure separates the upper and lower fields of V1. It is the only meridian representation that does not mark a border between different visual areas. As in the macaque, the borders between V1 and the two halves of V2 (V2d and V2v) are marked by vertical meridian representations, one just above (VMi1) and one below (VMs1) the calcarine sulcus. As pointed out by others (25), V2d and V2v together provide a second complete representation of the visual hemifield. However, it is split in half with the inferior field represented dorsally and the superior field represented ventrally.

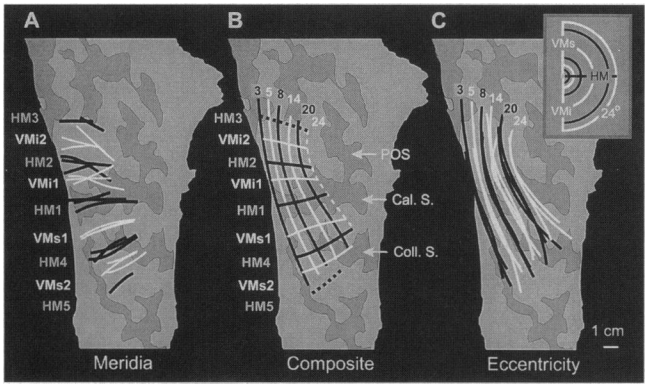

FIG. 3. Combined visual field topography for three subjects. Spline curves manually fit to major bands of activation on each subject's flat map were coregistered by simple affine transformations (maximum 10% scaling, 5° rotation). (*A*) Correspondence of meridian representations. Meridia were assumed to correspond approximately to middle of activity bands in Fig. 2. (*B*) Composite mean retinotopic grid. (*C*) Correspondence of isoeccentricity contours. All grids were superimposed on the sulcal pattern of subject A in Figs. 1 and 2. Dashed meridian contours in *B* were not observed in all subjects. Dashed eccentricity contour in *B* is only approximate due to maximum viewable eccentricity (30°). HM1–HM5, horizontal meridian representations; VMi1-2 and VMs1-2, inferior and superior vertical meridian representations.

Additional representations of the horizontal meridian mark the border between V2d and V3 dorsally (HM2) and between V2v and VP ventrally (HM4). Together, areas V3 and VP make up a third hemifield representation. However, in the macaque, these two quarter-field maps contain neurons with somewhat different visual response properties and anatomical connections (26). As a result, they were given different names by some investigators. Others have preferred to emphasize that they form a complete hemifield representation and so have termed them V3d and V3v (27).

The dorsolateral border of V3 is an inferior vertical meridian representation (VMi2). In the macaque, this would form the border with area V3A, at least for visual field eccentricities within 10° of the fovea (1, 26). Consequently, we have tentatively called this area V3A in the human. However, some investigators have argued that parts or all of macaque V3 and V3A should be considered a single dorsomedial area, DM (24). In either case, V3A (or DM) in monkeys contains both an inferior and superior quadrant representation. In the human, the corresponding superior quadrant representation that should be in dorsal cortex is missing. (Though, a weak focus of superior quadrant activity can sometimes be seen just posterior to the parietooccipital sulcus and dorsal to the calcarine sulcus—see Fig. 2).

The ventrolateral border of area VP (V3v) is formed by a second representation of the superior vertical meridian (VMs2). In the macaque, this forms the border between areas VP and the ventral portion of V4. So, we have called this area V4v in the human. The location of V4v corresponds to some of the locations identified in positron emission tomography studies as having color-selective responses (2). However, there is sufficient variability to make it difficult to be certain that such responses could not have come from VP.

Laterally at the junction of the parietal, occipital, and temporal lobes is another visually responsive region that has a representation emphasizing the peripheral visual field (>10°). We and others (28) have shown that this region contains neurons that are strongly responsive to movement. We concur with previous studies identifying this region as containing at

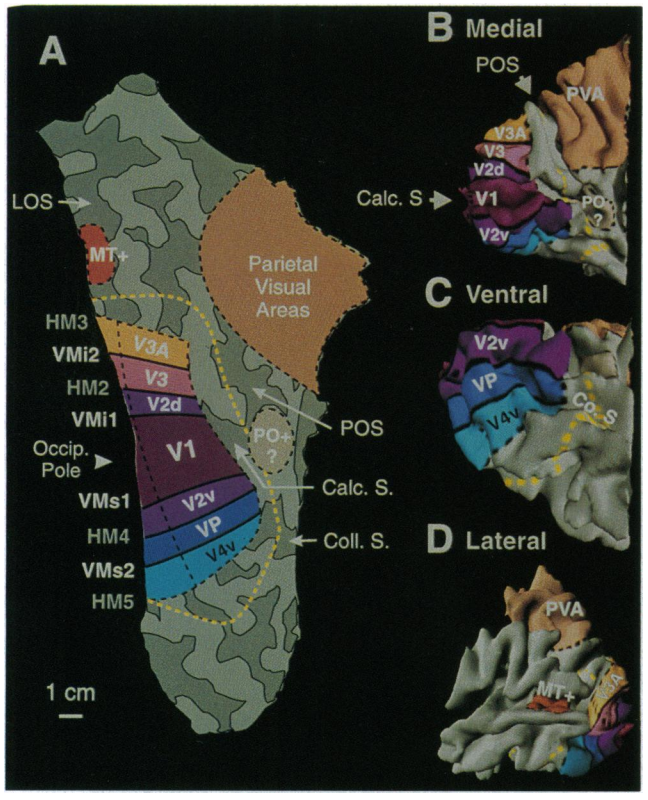

FIG. 4. Proposed topography of human visual areas shown on flat map and three-dimensional model of occipital lobe. Visual area nomenclature from Felleman and Van Essen (1). V1, primary visual cortex; V2d and V2v, dorsal and ventral divisions of second visual area; V3, third visual area; VP, ventroposterior visual area; V3A, visual area 3A; V4v, ventral division of fourth visual area. Other abbreviations are defined in Fig. 2. Yellow dotted line, maximum extent of activation.

least one area homologous to the middle temporal area in macaques (2, 3, 8). The apparent emphasis of the peripheral visual field representation in this region is consistent with the middle temporal area. However, it should be noted that in the macaque, the middle temporal area is surrounded by several additional small motion-responsive areas including V4t, the medial superior temporal area, and the fundus of the superior temporal sulcus (area FST) (29). So, we prefer to call this region the middle temporal complex (MT+) pending clarification by additional experiments.

Another consistent focus that was activated mainly by peripheral annuli was located in or near the parietooccipital sulcus, anterior to V1 and V2d. The topography and location of this area suggest that it could be homologous to the parietooccipital area in the macaque (22), but these characteristics alone do not permit a definite identification. Several other foci in dorsal parietal cortex were also activated strongly by stimulation of the peripheral visual field. In the macaque, parietal cortex contains several functionally distinct visual areas, all of which tend to be dominated by peripheral field representations. Since the exact locations of parietal foci in these experiments were variable, it would be premature to identify any of these sites with specific visual areas in the macaque.

In order to facilitate comparison of the results presented here with previous work, Fig. 5 illustrates the flat map of human visual areas together with matching maps calibrated in the standardized coordinate system of Talairach and Tournoux (30). The Talairach coordinates of any feature on the map of visual areas can be easily determined if the reader traces the feature and the outline of the map onto a transparent sheet. The sheet can then be aligned over each calibration map in turn. The intersection of the feature with a contour on each map gives the *x*, *y*, and *z* Talairach coordinates.

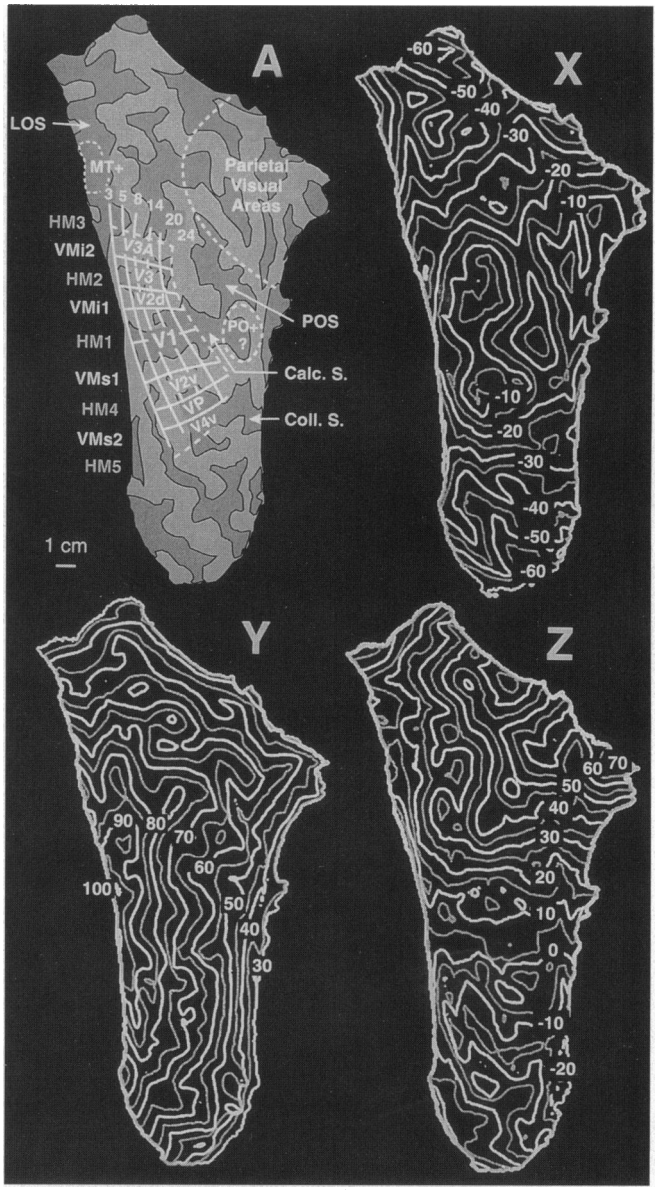

FIG. 5. Standardized Talairach coordinate system for flat map of human visual areas. (*A*) Proposed human visual areas (see Fig. 4). X, Y, and Z are maps calibrated in the coordinate system of Talairach and Tournoux (30). Contours represent loci of constant *x*, *y*, and *z* coordinates, respectively. Note that *y* coordinates are positively increasing in posterior direction in accord with the American College of Radiology proposed standard (31). LOS, lateral occipital sulcus. Other abbreviations are as in Figs. 2 and 4.

DISCUSSION

The retinotopic maps shown here indicate that there is a consistent retinotopic organization of visually responsive cortex throughout much of the human occipital lobe, especially medially and ventrally. Within this region, isoeccentricity contours run more or less orthogonally to the isoangular contours (Fig. 3*B*). There are at least three more or less complete representations of the contralateral visual hemifield as well as several partial representations within the cortex activated by these experiments. By analogy with the topography of visual areas in the macaque monkey, at least six distinct visual areas can be identified in additional to the primary visual cortex, V1.

Visually responsive areas in parietal cortex can be detected but cannot, as yet, be positively identified.

The present results are consistent with the map of a single subject illustrated by Sereno *et al.* (11), though the present results show mapping of mean eccentricities up to 24° from the fovea, nearly twice that of previous MRI studies. The comparison across subjects presented here shows that the topography of visual areas can be highly consistent across subjects. However, the correspondence between visual area boundaries and gyral landmarks in individual subjects can vary. For instance, the border between areas VP and V4v can be on the medial side of the collateral sulcus in one subject but on the lateral side of the sulcus in another. Such individual variation can be of paramount significance for potential clinical applications such as presurgical planning. It also poses important methodological concerns for imaging studies that rely on averaging across subjects to enhance sensitivity. Although the standardized coordinate system of Talairach and Tournoux provides a means for comparing the present results with other studies, caution should be exercised in drawing conclusions about the correspondence between functionally identified sites and specific visual areas unless the topography for each individual has been mapped.

Note Added in Proof. In agreement with our speculation in the text, a quantitative analysis of results from several PET studies suggests that the site we have designated as MT+ is likely to be a subdivision (MST) of the more extensive complex of motion areas in lateral occipital cortex.

We thank Jon Wieser for expert technical assistance. E.A.D. also expresses his gratitude to Dr. Carman for collaborating on this project and making the unfolding algorithm available. This work was supported by National Institutes of Health Grants EY10244 and MH51358 and by Core Grant EY01931.

1. Felleman, D. J. & Van Essen, D. C. (1991) *Cereb. Cortex* **1,** 1–148.
2. Zeki, S., Watson, J. D. G., Lueck, C. J., Friston, K. J., Kennard, C. & Frackowiak, R. S. J. (1991) *J. Neurosci.* **11,** 641–649.
3. Tootell, R. B. H., Reppas, J. B., Kwong, K. K., Malach, R., Born, R. T., Brady, T. J., Rosen, B. R. & Belliveau, J. W. (1995) *J. Neurosci.* **15,** 3215.
4. Clarke, S. & Miklossy, J. (1990) *J. Comp. Neurol.* **298,** 188–214.
5. Horton, J. C. & Hoyt, W. F. (1991) *Arch. Ophthalmol.* **109,** 816–824.
6. Tootell, R. B. H. & Taylor, J. B. (1995) *Cereb. Cortex* **1,** 39–55.
7. Lueck, C. J., Zeki, S., Friston, K. J., Deiber, M. P., Cope, P., Cunningham, V. J., Lammertsma, A. A., Kennard, C. & Frackowiak, R. S. J. (1989) *Nature (London)* **340,** 386–389.
8. Corbetta, M., Miezin, F. M., Dobmeyer, S., Shulman, G. L. & Petersen, S. E. (1991) *J. Neurosci.* **11,** 2383–2402.
9. Haxby, J. V., Horwitz, B., Ungerleider, L. G., Maisog, J. M., Pietrini, P. & Grady, C. L. (1994) *J. Neurosci.* **14,** 6336–6353.
10. Orban, G. A., Dupont, P., De Bruyn, B., Vogels, R., Vandenberghe, R. & Mortelmans, L. (1995) *Proc. Natl. Acad. Sci. USA* **92,** 993–997.
11. Sereno, M. I., Dale, A. M., Reppas, J. B., Kwong, K. K., Belliveau, J. W., Brady, T. J., Rosen, B. R. & Tootell, R. B. H. (1995) *Science* **268,** 889–893.
12. DeYoe, E. A., Bandettini, P., Neitz, J., Miller, D. & Winans, P. (1994) *J. Neurosci. Methods* **54,** 171–187.
13. DeYoe, E. A., Neitz, J., Miller, D., Winans, P., Glickman, S. & Wieser, J. (1994) *Invest Ophthalmol. Visual Sci.* **35,** 1813.
14. DeYoe, E. A., Miller, D., Winans, P. & Neitz, J. (1994) *Soc. Neurosci. Abstr.* **20,** 840.
15. Engel, S. A., Wandell, B. A., Rumelhart, D. E., Lee, A. T., Shadlen, M. N., Chichilinsky, E. J., Glover, G. H. & Newsome, W. T. (1993) *Soc. Neurosci. Abstr.* **19,** 335.
16. Wong, E. C., Bandettini, P. A. & Hyde, J. S. (1992) *Proc. Soc. Magn. Reson. Med.* **1,** 105.
17. DeYoe, E. A., Neitz, J., Miller, D. & Wieser, J. (1993) *Proc. Soc. Magn. Reson. Med.* **3,** 1394.
18. Bandettini, P. A., Jesmanowicz, A., Wong, E. C. & Hyde, J. S. (1993) *Magn. Reson. Med.* **30,** 161–173.
19. Hays, W. L. (1973) *Statistics for the Social Sciences* (Holt, Rinehart & Winston, New York).
20. Geiger, B. (1993) Ph.D. thesis (École des Mines de Paris).
21. Carman, G. J. (1990) Ph.D. thesis (California Institute of Technology, Pasadena, CA).
22. Colby, C. L., Gattass, R., Olson, C. R. & Gross, C. G. (1988) *J. Comp. Neurol.* **269,** 392–413.
23. Van Essen, D. C., Felleman, D. J., DeYoe, E. A., Olavarria, J. & Knierim, J. (1990) *Cold Spring Harbor Symp. Quant. Biol.* **55,** 679–696.
24. Kaas, J. H. & Krubitzer, L. A. (1991) in *Vision and Visual Dysfunction: Neuroanatomy of the Visual Pathways and their Development*, eds. Dreher, B. & Robinson, S. R. (CRC, Boca Raton, FL), Vol. 3, pp. 302–323.
25. Allman, J. M. & Kaas, J. H. (1974) *Brain Res.* **76,** 247–265.
26. Burkhalter, A., Felleman, D. J., Newsome, W. T. & Van Essen, D. C. (1986) *Vision Res.* **26,** 63–80.
27. Boussaoud, D., Ungerleider, L. G. & Desimone, R. (1990) *J. Comp. Neurol.* **296,** 462–495.
28. Beauchamp, M. S. & DeYoe, E. A. (1995) *Soc. Neurosci. Abstr.*, **21,** 1760.
29. Ungerleider, L. G. & Desimone, R. (1986) *J. Comp. Neurol.* **248,** 190–222.
30. Talairach, J. & Tournoux, P. (1988) *Co-Planar Stereotaxic Atlas of the Human Brain* (Thieme Medical Publishers, New York).
31. ACR-NEMA Committee, W. G. V. (1993) (American College of Radiology, National Electrical Manufacturers Association, Washington, DC).